7. BIO-GEOCHEMISTRY (BGC)

Katharina Abrahamsson[1], Michael Angelopoulos[2], Dorothea Bauch[3], Josefa Verdugo[2] and Lei Wang[4]

[1]SE.GU
[2]DE.AWI
[3]DE.GEOMAR
[4]CN.BNU

Grant-No. AWI_PS122_00

A comprehensive summary of the bio-geochemical measurements during all 5 cruise legs will be published in the *Special Feature: The Multidisciplinary Drifting Observatory for the Study of Arctic Climate (MOSAiC)* of the scientific journal *Elementa: Science of the Anthropocene* (https://online.ucpress.edu/elementa/collection/269/Special-Feature-The-Multidisciplinary-Drifting)

Objectives

We plan a year-round process-level observation of climate relevant trace gases (CRTG) during the drift. The coupling of ice and snow physics on one side with the ecosystem on the other side includes numerous biogeochemical reactions during freezing and melting cycles of sea ice. This results in CRTG exchange with both the overlying atmospheric boundary layer and the underlying ocean down to the halocline. Quantifying seasonally varying fluxes is essential for future improvements of climate models. The understanding of the processes behind the observed CRTG fluxes requires a detailed knowledge of biochemistry, sea ice growth, and movement. The collected data links to most of the measurements in the atmosphere, snow, sea ice, ocean, and ecosystem domains.

Work at sea

We have measured dissolved gases (halocarbons, VHOC, CH_4 and $\delta^{13}C$-CH_4) in discrete samples of sea ice, snow, sea water, and brine. In addition, CH_4, $\delta^{13}C$-CH_4, CO_2 and halocarbons have been measured continuously in the atmosphere and surface water. Samples for stable water (H_2O) isotopes ($\delta^{18}O/\delta D$), Be, nutrients, Nd isotopes and I^- were also collected (Table 7.1-7.3). In total, 154 ice cores were collected and 90 snow samples (Table 7.1, 7.2). Furthermore, water was collected weekly from the rosette samplers at Ocean City and *Polarstern* (Table 7.3). The measurements of halocarbons, CH_4 and $\delta^{13}C$-CH_4, were performed on board and the other parameters will be analyzed at a later stage. Refer the Expedition Program for principal investigators and their scientific objective.

The atmospheric concentrations of BrO and IO were measured with a MAX DOAS from the start (exit of Russian EEZ) to the point of too low solar radiation.

The sites that were sampled for sea ice and snow are indicated in Figure X. Newly frozen seawater was sampled at BGC1 and at the first-year ice site in the dark sector (FYI Monday coring – cross-cutting theme). Second-year ice was sampled at BGC2, BGC3 and at the second-year site in the dark sector (SYI Monday coring – cross-cutting theme). Rafted ice was recovered at the second-year ice site, as well as at BGC2, BGC3, and in the logistics area. Site BGC2 was highly heterogeneous and also featured a refreezing freshwater pocket in a low relief area.

Tab.7.1: Ice coring events with sampled parameters

date	dship stat.nr.	Position	VHOC	CH_4	^{18}O	$\delta^{13}C$-CH_4	Be	N_2O
09.10.2019	PS122/1_2-95	lead	x	x	x			
10.10.2019	PS122/1_2-108	lead	x	x	x			
11.10.2109	PS122/1_2-109	lead	x	x	x			
14.10.2019	PS122/1_2_132	survey	x	x	x			
15.10.2019	PS122/1_2-134	lead	x	x	x			
18.10.2019	PS122-1_2-154	survey	x					
23.10.2019	PS122-1_2-203	survey	x	x	x			
24.10.2019	PS122-1_4-29	BGC_1	x	x	x			
28.10.2019	PS122-1_5-3	FYI_mc	x	x	x		x	x
28.10.2019	PS122-1_5-78	SYI_mc	x	x	x	x		x
28.10.2019	PS122-1_5-81	RAFT	x	x	x	x		
30.10.2019	PS122-1_5-24	BGC_1	x	x	x			
02.11.2019	PS122/1_5-68	BGC_2	x	x	x			
04.11.2019	PS122-1_6-34	FYI_mc	x	x	x		x	x
04.11.2019	PS122-1_6-36	SYI_mc	x	x	x			x
04.11.2019	PS122-1_6-10	RAFT	x	x	x			
06.11.2019	PS122-1_6_59	BGC_3	x	x	x			
07.11.2019	PS122-1_6_61	BGC_1	x	x	x			
10.11 2109	PS122/1_6-135	BGC_2	x	x	x			
11.11.2019	PS122/1_7-6	FYI_mc	x	x	x		x	x
11.11.2019	PS122/1_7-9	SYI_mc	x	x	x			x
11.11.2019	PS122/1_7-112	RAFT						
13.11.2019	PS122/1_7-52	BGC_3	x	x	x			
14.11.2019	PS122/1_7-78	BGC_1	x	x	x	x		
15.11.2019	PS122/1_7-94	BGC_2	x	x	x			
16.11.2019	PS122/1_7-97	FYI_mc					x	
18.11.2019	PS122/1_8-2	FYI_mc	x	x	x		x	
19.11.2019	PS122/1_8-22	BGC_1	x					
19.11.2019	PS122/1_8-22	BGC_1	x	x	x			
20.11.2019	PS122/1_8-37	BGC_2	x	x	x			
20.11.2019	PS122/1_8-74	BGC_2 FW	x	x	x			
23.11.2019	PS122/1_8-111	BGC_2 FW	x	x	x	x		
25.11.2019	PS122/1_9-6	FYI_mc	x	x	x	x	x	x
25.11.2019	PS122/1_9-11	SYI_mc	x	x	x			x
25.11.2019	PS122/1_9-30	RAFT	x	x	x			
27.11.2019	PS122/1_9-40	BGC_1	x	x	x			
28.11.2019	PS122/1_9-63	BGC_2	x	x	x			
30.11.2019	PS122/1_9-97	BGC_2	x	x	x			
02.12.2019	PS122/1_10-16	SYI_mc	x	x	x		x	x
02.12.2019	PS122/1_10-19	FYI_mc	x	x	x			x
04.12.2019	PS122/1_10-39	BGC_1	x	x	x			
06.12.2019	PS122/1_10-69	BGC_3	x	x	x			
10.12.2019	PS122/1_11-11	BGC_1						

Tab 7.2: Snow sampling events with sampled parameters

date	dship stat.nr.	Position	VHOC	CH_4	^{18}O	Be	$\delta^{13}C$-CH_4
24.10.2019	PS122/1_4-44	BGC_1	x			x	
28.10.2019	PS122/1_5-92	FYI_mc	x	x	x		
28.10.2019	PS122/1_5-93	SYI_mc	x	x	x		
30.10.2019	PS122/1_5-94	BGC_1	x				
30.10.2019	PS122/1_5-5		x				
31.10.2019	PS122/1_5-90	BGC_1					x
02.11.2019	PS122/1_5-95	BGC _2	x	x	x		
02.11.2019	PS122/1_5-91	BGC_2					x
04.11.2019	PS122/1_6-138	FYI_mc	x				
04.11.2019	PS122/1_6-139	SYI_mc	x				
04.11.2019	PS122/1_6-133	SYI_mc					x
06.11.2019	PS122/1_6-140	BGC_3	x		x		
06.11.2019	PS122/1_6-134	BGC_3					x
07.11.2019	PS122/1_6-141	BGC_1	x	x	x		
10.11 2109	PS122/1_6-136	BGC_2	x	x	x		
11.11.2019	PS122/1_7-105	FYI_mc	x				
11.11.2019	PS122/1_7-106	SYI_mc	x				
13.11.2019	PS122/1_7-51	BGC_3	x		x		
13.11.2019	PS122/1_7-131	BGC_3					x
14.11.2019	PS122/1_7-74	BGC_1	x	x			
14.11.2019	PS122/1_7-75	BGC_1					x
15.11.2019	PS122/1_7-89	BGC_2	x	x	x		
15.11.2019	PS122/1_7-91	BGC_2					x
19.11.2019	PS122/1_8-24	BGC_1	x	x		x	x
19.11.2019	PS122/1_8-10	BGC_1					x
20.11.2019	PS122/1_8-33	BGC_2	x	x	x		
20.11.2019	PS122/1_8-35	BGC_2 FW					x
23.11.2019	PS122/1_8-110	BGC_2 FW	x	x	x		
25.11.2019	PS122/1_9-4	FYI_mc	x	x	x		
25.11.2019	PS122/1_9-31	SYI_mc	x	x	x		
25.11.2019	PS122/1_9-8	SYI_mc					x
26.11.2019	PS122/1_9-23	snow 1	x		x		
27.11.2019	PS122/1_9-39	BGC_1	x				
28.11.2019	PS122/1_9-65	BGC_2	x	x	x		
28.11.2019	PS122/1_9-68	BGC_2					x
30.11.2019	PS122/1_9-95	BGC_2	x	x	x		
02.12.2019	PS122/1_10-35	SYI_mc	x	x	x		
02.12.2019	PS122/1_10-10	FYI_mc	x	x	x		
02.12.2019	PS122/1_10-5		x		x		
02.12.2019	PS122/1_10-9	SYI_mc					x
04.12.2019	PS122/1_10-38	BGC_1	x				
04.12.2019	PS122/1_10-40	BGC_1	x				x
05.12.2019	PS122/1_10-47	BGC_2 FW	x	x	x		
06.12.2019	PS122/1_10-81	BGC_3					
06.12.2019	PS122/1_10-68	BGC_3					x
10.12.2019	PS122/1_11-12	BGC_1					

Tab.7.3: Water sampling events with sampled parameters

date	dship stat.nr.	Position	VHOC	CH_4	^{18}O	$\delta^{13}C$-CH_4	N_2O	nutr	I^-	Nd
04.10.2019	PS122/1_2-68	PS	x	x	x					x
24.10.2019	PS122-1_4-37	Ocean City	x	x	x			x		x
31.10.2019	PS122/1_5-40	Ocean City	x							
01.11.2019	PS122-1_5-46	Ocean City	x	x	x	x	x		x	
07.11.2019	PS122-1_6-38	Ocean City	x	x	x	x				
08.11.2019	PS122/1_6-58	PS	x							
13.11.2019	PS122-1_7-40	Ocean City	x	x	x		x			
14.11.2019	PS122/1_7-49	PS	x							
19.11.2019	PS122-1_8-16	Ocean City	x	x	x	x	x	x		
26.11.2019	PS122/1_9-48	Ocean City	x	x	x	x		x	x	
28.11.2019	PS122/1_9-50	PS	x							
30.11.2019	PS122/1_9-87	PS								x
03.12.2019	PS122/1_10-26	Ocean City	x	x	x		x			
05.12.2019	PS122/1_10-45	Ocean City	x	x	x		x			
05.12.2019	PS122/1_10-64	PS	x							
12.12.2019	PS122/1_11-40	Ocean City	x	x	x	x		x		

Air-ice flux chamber measurements

As part of the trace gas ice coring program, the BGC team deployed CO_2 and CH_4 gas flux chambers at multiple sites. By deploying chambers on various ice types throughout the year, we hypothesize that we will able to see how permeable atmosphere-ice and atmosphere-snow-ice systems are to gas fluxes as the snow and ice conditions change. The device first measures atmospheric CO_2 and CH_4 concentrations and then measures the gas concentrations over time in an isolated space by circulating air from the chamber to the Los Gatos analysers. If the gas concentrations increase or decrease, this suggests a flux out of or into the snow or ice boundary. By taking ice cores alongside our chamber deployments, we may be able to relate the evolving temperature and salinity regimes of the ice to gas fluxes.

The chamber was deployed at BGC1 (first year ice), BGC3 (second-year ice), as well as the second-year ice and refreezing water pocket plots at BGC2. Ideally, the chamber was deployed on both ice and snow surfaces to assess fluxes at air-ice and air-snow boundaries. For each deployment, the operators recorded the surface conditions, chamber setup configuration, as well as the wind speed and direction. When possible, the chamber was set up upwind of *Polarstern*, the coring site, and any other nearby activities to avoid contamination. At sites BGC2 (second-year ice plot) and BGC3, Team Atmosphere deployed its chamber on the snow surface for comparison. A summary of the deployments is provided in Table 7.4 and an example of dual chamber deployment is shown in Figure 7.1.

Tab.7.4. Summary of Gas Flux Chamber Deployments

Site	Device Operation	Date	Deployment on Ice Surface	Deployment on Snow Surface	Comment
BGC1	PS122/1-4-28	2019-10-24	x	x	Tube to chamber connection failure

BGC1	PS122/1_5-71	2019-10-31	x	x	Ice surface measurements are suspicious.
BGC3	PS122/1_7-50	2019-11-13		x	Team Atmosphere deployed its chamber on snow surface.
BGC2 SYI	PS122/1_8-67	2019-11-21	x	x	Team Atmosphere deployed its chamber on snow surface on 2019-11-20.
BGC2 Water Pocket	PS122/1_10-46	2019-12-05	x		Snowdrift partially buried chamber.

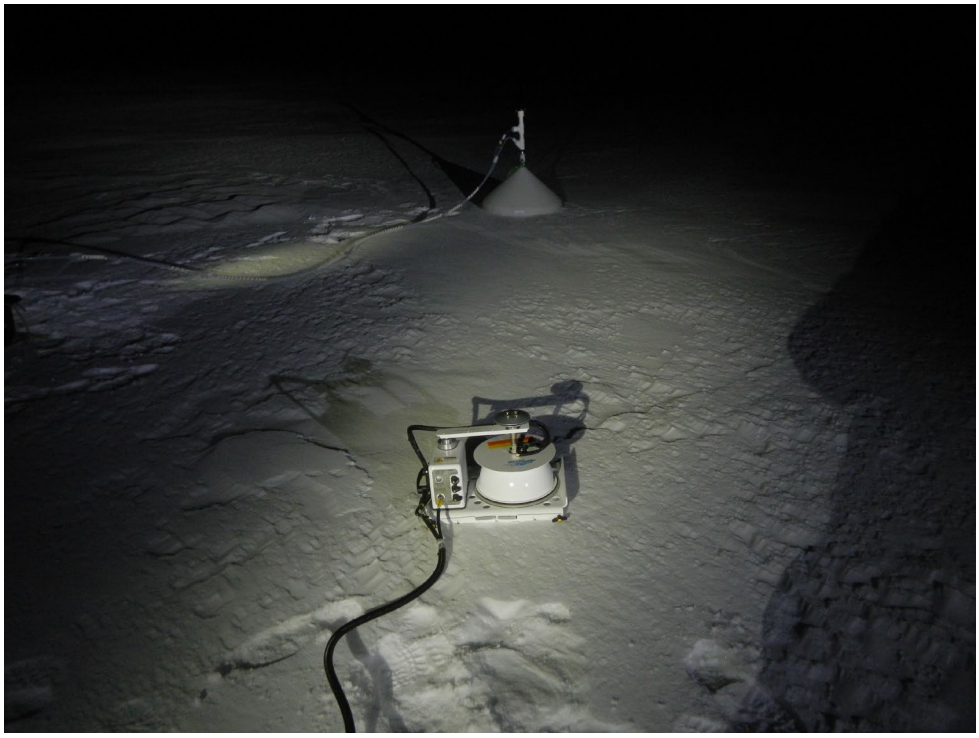

Fig.7.1: Dual chamber deployment at BGC3 on 2019-11-13

Surface water handheld CTD measurements

A handheld Sontek-CTD was deployed to the upper 30m of the surface waters (or within enclosed water pockets) through the coring holes during sea ice sampling at most coring sites (Table 7.5). The mobile CTD was used primarily to determine the thickness of the winter mixed layer and to extend the thermal and salinity regimes of the ice into the water column. The cast results for temperature and salinity at the SYI site in the dark sector are shown in Figure 7.2 and Figure 7.3, respectively.

Tab.7.5 Dates and sites of handheld Sontek CTD deployments.

date	dship stat.nr.	Position
23.10.2019	PS122/1_2-200	LOG area
24.10.2019	PS122/1_4-24	BGC_1
28.10.2019	PS122/1_5-19	SYI_mc
30.10.2019	PS122/1_5-41	BGC_1

02.11.2019	PS122/1_5-70	BGC_2
02.11.2019	PS122/1_5-69	BGC_2
04.11.2019	PS122/1_6-23	SYI_mc
06.11.2019	PS122/1_6-60	BGC_3
07.11.2019	PS122/1_6-62	BGC_1
10.11 2109	PS122/1_6-137	BGC_2
14.11.2019	PS122/1_7-76	BGC_1
15.11.2019	PS122/1_7-90	BGC_2
19.11.2019	PS122/1_8-25	BGC_1
20.11.2019	PS122/1_8-75	BGC_2
20.11.2019	PS122/1_8-76	BGC_2 FW
23.11.2019	PS122/1_8-109	BGC_2 FW
25.11.2019	PS122/1_9-9	SYI_mc
27.11.2019	PS122/1_9-35	BGC_1
28.11.2019	PS122/1_9-64	BGC_2
30.11.2019	PS122/1_9-96	BGC_2
02.12.2019	PS122/1_10-36	SYI_mc
04.12.2019	PS122/1_10-37	BGC_1
06.12.2019	PS122/1_10-83	BGC_3
10.12.2019	PS122/1_11-13	BGC_1

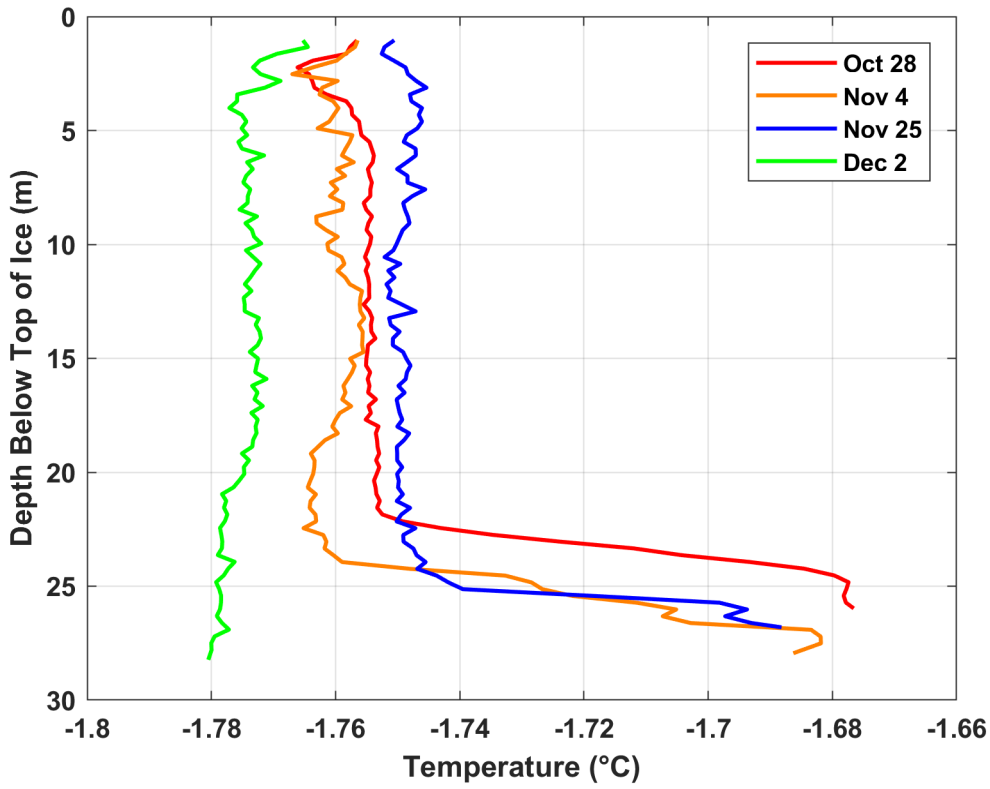

Fig.7.2: Temperature regimes in the water column at SYI site in the dark sector.

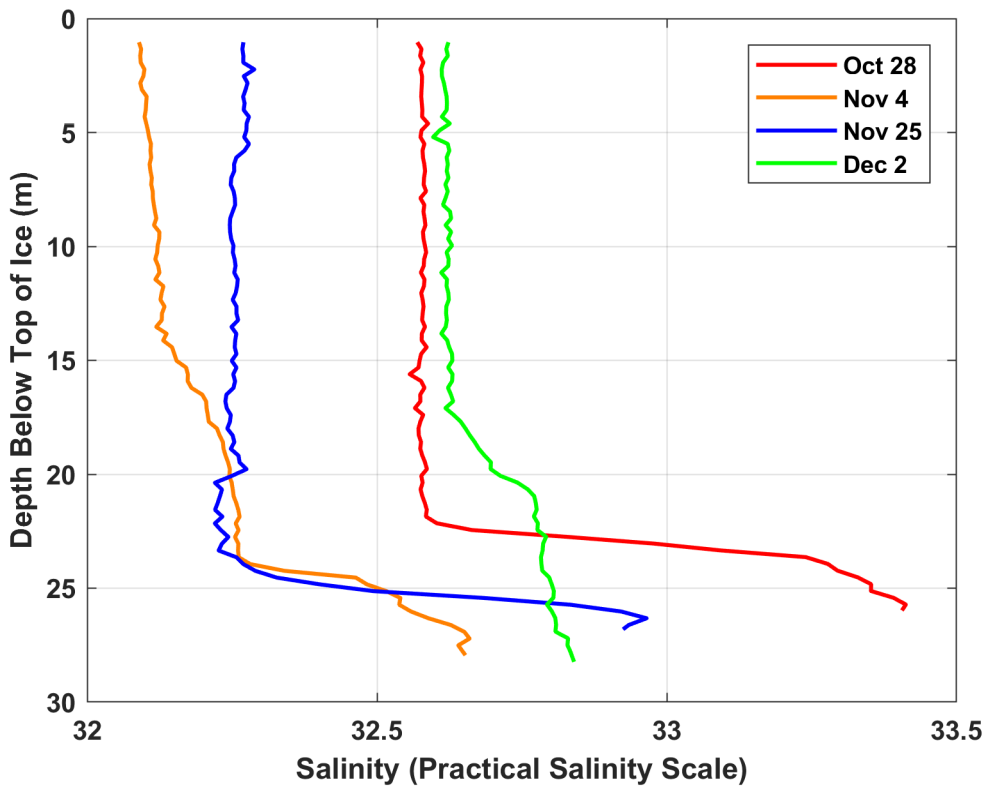

Fig.7.3: Salinity regimes in the water column at SYI site in the dark sector.

Overview of spatial variability.

A quick overview of the composition of halocarbons and methane at the different sites is given in Figure 7.4. The color scheme indicates the different sampling sites. As can be seen from this principal component analysis (PCA), the second-year ice site (SYI, blue) has a similar composition to that of BGC2 (green) as indicated by the score plot (Figure 7.5, top). The two first year ice sites (BGC1 (yellow) and FYI (black)) have compositions that are similar to each other. The main differences are indicated in the loading plot (Figure 7.4, bottom) with relatively higher concentrations of halocarbons in first-year ice and relatively higher concentrations of CH_4 in second year ice.

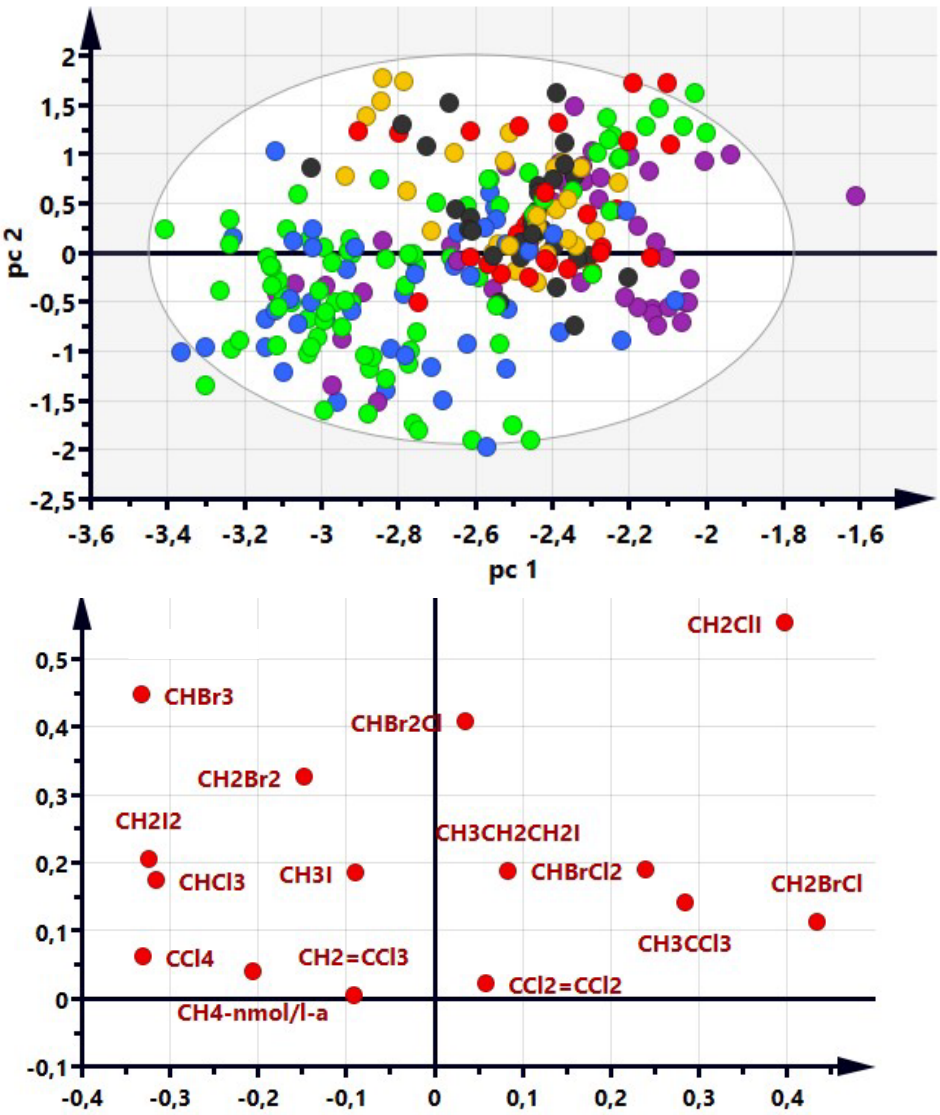

Fig.7.4: Halocarbon and CH_4 composition at the different sampling sites.

A principal component analysis (R2X = 0,949; Q2 = 0,87) based on 14 different VHOC and CH_4 and the six different sample sites were performed. The top graph is the scatter score plot with BGC1 – orange; BGC2 – green; BGC3 – red; FYI – black; SYI – blue; raft ice – purple. The bottom graph is the loading plot.

Data Management

All data are handled, documented, archived and published following the MOSAiC data policy (see APPENDIX). Final data products will be stored at the PANGAEA data repository (World Data Center PANGAEA Data Publisher for Earth & Environmental Science (www.pangaea.de)).

References

No references

7.1 Fate and pathways of methane in sea ice and surface water

Josefa Verdugo[1], Michael Angelopoulos[1], Dorothea Bauch[2]
(not on board:) Ellen Damm[1]

[1]DE.AWI
[2]DE.GEOMAR

Objectives

Elevated atmospheric methane concentrations over open leads and regions with fractional sea ice cover (Korts et al., 2012) point to sea ice implications in the role of transferring methane from the oceans to the atmosphere. A cascade of feedback processes triggered by freezing and melting events of sea ice induces seasonally the uptake of methane from sources remote from the locations where methane is released (Damm et al., 2015, 2018). We considered the following pathways: direct interactions, i.e. from ice and snow to surface water and indirect interactions, where trace gases circulate through more than one environment before leaving to the atmosphere. Hence, our project is closely linked to the planned detailed seasonal tracing of sea-ice processes by stable water isotopes H_2O ($\delta^{18}O$ and δD). We focus on alterations in the isotopic composition of methane along these pathways mainly by the kinetic isotopic fractionation effect. This fractionation may lead to modifications of the isotopic signature compared to the initial source signature, which are not considered yet. Those processes might encourage a misinterpretation and finally misleading source identification of the Arctic emissions.

Work at sea

During leg 1 of MOSAiC, we measured CH_4 concentration and the $\delta^{13}C$ signature of methane in surface waters and sea ice. Samples for stable isotopes of H_2O ($\delta^{18}O$ and δD) were always taken in parallel for later analysis (see Tables 7.1-7.3).

Seawater sampling occurred from the Ocean City rosette weekly. This schedule aims to collect a year-round time series for the trace gas budget calculation. Sampling in the upper 100 m was carried out with the highest vertical resolution in the sea ice-affected water while below this horizon at standard 50 m depths down to 300 m or the inflowing Atlantic water.

The sampling depths were adapted depending on the CTD profile, i.e. structure of the water column. Sea ice was sampled by taking cores with a standard Kovacs 9 cm ice corer. Afterwards, the ice cores were sectioned in 10 cm pieces in the 0 °C container and melted at ~15°C in gas tight bags. Methane concentration was measured on board by a gas chromatography (GC) device equipped with a flame ionization detector (FID). The $\delta^{13}C$ signature of methane was analyzed with a PICARRO 2132 on board.

Preliminary results

Methane concentration in surface waters

During the ice drift, the waters underneath the sea ice (upper 100 m) were slightly undersaturated in methane, relative to the atmospheric background (see Figure 7.5). The saturation relative to the atmospheric equilibrium was calculated from the mean concentration of the triplicates or duplicates samples using the CTD temperature and salinity values at the corresponding depth.

Methane concentration in sea ice

Methane concentrations were was measured in different type of sea ice: FYI, SYI and Rafted ice to have an overview about the spatial variability in our ice floe. FYI contained methane concentration in the same range of magnitude as the waters underneath the sea ice, resulting from the methane up-taken during the ice growth (Figure 7.6),

In second year ice, (refrozen melt pond) methane concentrations exhibit values similar to those found in FYI. The exception was found in rafted or ridged ice, where higher methane concentrations (up to 6 nM) in comparison to FYI and SYI were observed.

By combining year-round observations we will be able to evaluate how seasonal variability in physical and biogeochemical regimes affect trace gas distribution and sea/ice air fluxes.

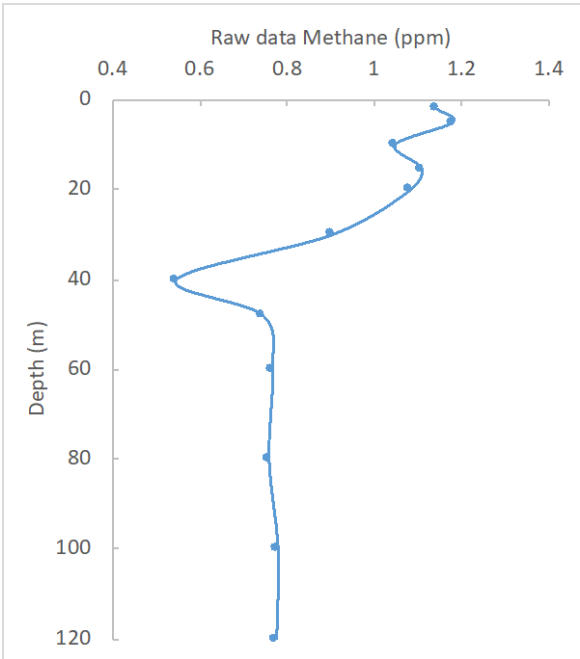

Fig.7.5: Methane profile taken at the Ocean City CTD during 26th of November, 2019. The methane undersaturated waters at the surface show a disconnection between the atmosphere and the surface ocean.

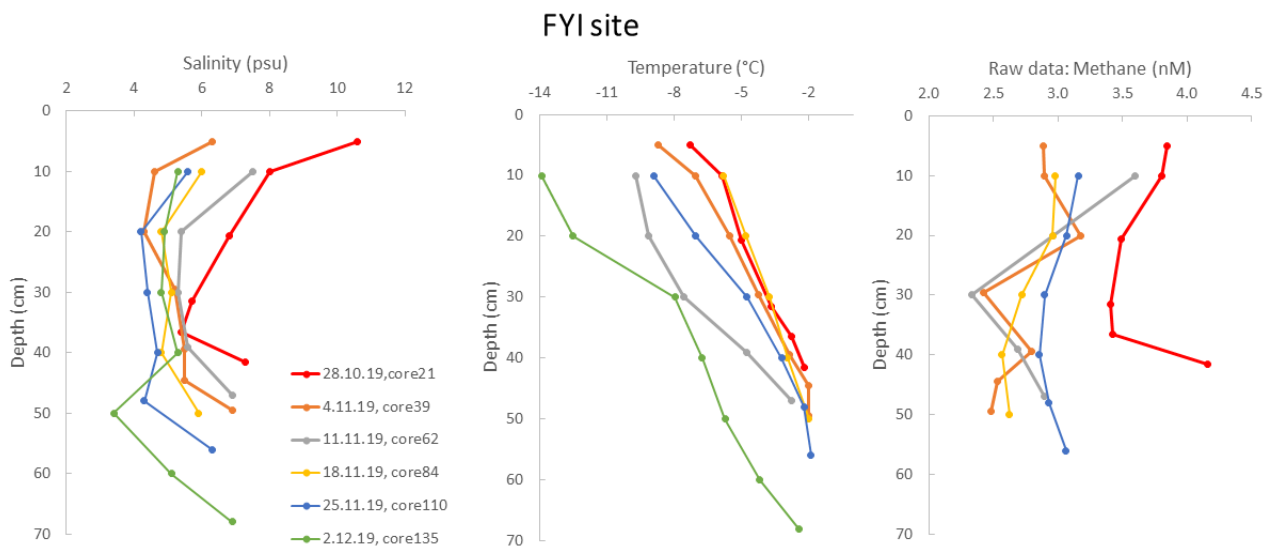

Fig.7.6: Temporal evolution of methane concentration in response to salinity and temperature changes in first-year ice sampled at the Monday coring – cross-cutting site.

Data management

All data are handled, documented, archived and published following the MOSAiC data policy (see APPENDIX). Final data products will be stored at the PANGAEA data repository (World Data Center PANGAEA Data Publisher for Earth & Environmental Science (www.pangaea.de)).

References

Damm, E., Rudels ,B., Schauer, U., Mau, S. and Dieckmann, G., 2015: Methane excess in Arctic surface water- triggered by sea ice formation and melting. Scientific Reports 5:16179, doi: 10.1038/srep16179

Damm, E., Bauch, D., Krumpen, T., Rabe, B., Korhonen, M., Vinogradova, E. and Uhlig, C. 2018: The Transpolar Drift conveys methane from the Siberian shelf to the central Arctic Ocean. Scientific Reports 8:4515, doi: 10.1038/s41598-018-22801-z

Kort, S. C., Wofsy, B. C., Daube, M., Diao, J. W. Elkins, et al. 2012: Atmospheric observation of Arctic Ocean methane emissions up to 82°N. Nature geosciences, doi.org/10.1038/NGEO1452

7.2 *In situ* measurements (CH_4, N_2O, CO and CO_2) in sea water and air

Lei Wang[1] [1]CN.BNU

(not on board:) Cunde Xiao[1], Zhiheng Du[2] [2]CN.NIEER.CAS

Objectives

1. A sustained decline of sea ice extent was observed in the Arctic Ocean over the past few decades, which may have significant impact on CH_4 and CO_2 exchange between the ocean and the atmosphere. This may affect global carbon cycles by enhancing the sea-air flux to the atmosphere. In addition, sea ice absorbs methane in the atmosphere by photochemical and biochemical oxidation. However, the impact is still not well understood. With the increase of global atmospheric temperature and the melting of Arctic sea ice, sea ice's role of shielding and consumption of greenhouse gas is weakening. Thus, this area may turn into an important source of atmospheric CH_4, which can have a significant impact on regional and global carbon cycles and climate systems. Therefore, we aim to quantitatively estimate the amount of greenhouse gases in the Arctic Ocean through large-scale underway observations. Specific questions include: 1) How does greenhouse gas (GHG) concentration in the surface sea water change when the ice is growing?; 2) How does GHG concentration change in spring when the ice is melting?

2. Dust sources are mainly distributed in middle latitude arid and semi-arid regions. To date, many studies have concentrated on the analysis of dust sources in arid and semi-arid regions based on geochemical tracers. In particular, the transport of mineral dust from East Asian deserts is global in scale. To further link the dust transport relationship between the middle latitude and High Arctic regions, further study is needed to assess the impact of mineral dust transported from lower latitude deserts on the dust variations in high latitude regions. Therefore, we aim to take some snow samples to measure the stable isotopic ratios of strontium (Sr), neodymium (Nd), and lead (Pb) in insoluble dust in snow samples. The results from the snow samples will be compared to those of soil and sand samples from East Asia.

Work at sea

Surface sea water greenhouse gas

The Arctic Ocean surface water methane and carbon dioxide fluxes, as well as methane and carbon dioxide isotope were measured concurrently using an integrated nozzle-type equilibrator (EQ) and cavity ring-down spectrometer (CRDS) enabling high spatial resolution measurements (Figure 7.7). Stable carbon isotope values measured with the Picarro-2201i were calibrated against standard gases to obtain accurate $\delta^{13}C$ values of surface water methane (±4‰ at 2 ppm; ±1.5‰ at 5 ppm) and CO_2 (±1.5‰). The gas concentration data were combined with meteorological (wind speed, air temperature), equilibrator temperature, and sea surface water environmental parameters (salinity, water temperature). The system is continuously running in the Fishlab (Figure 7.8).

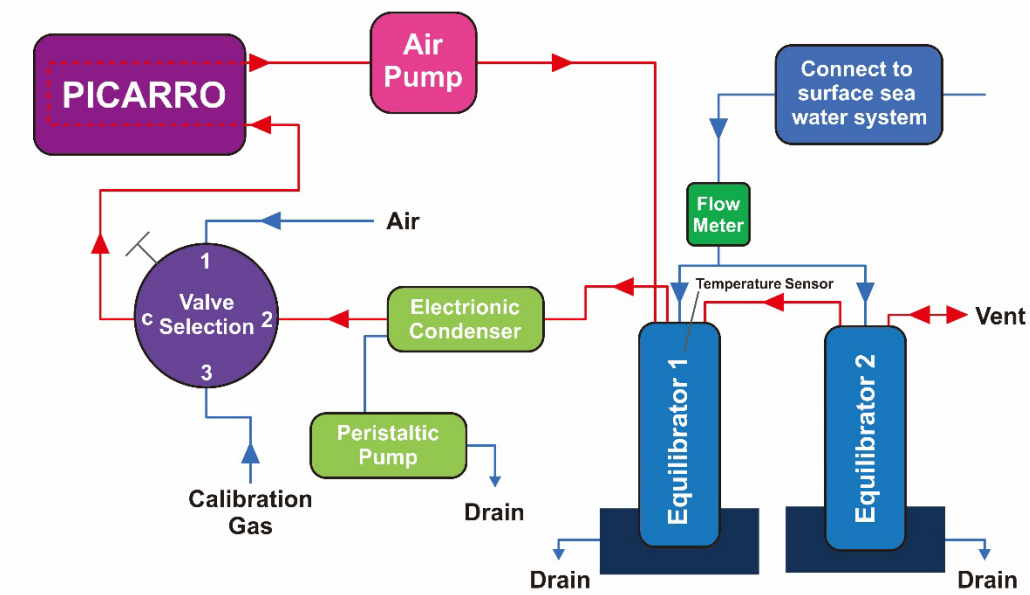

Fig.7.7: Integrated double nozzle-type equilibrator and cavity ring-down spectrometer (CRDS): the equilibrator mode (blue), the equilibrium gas loop mode (red line), the dryer mode (green), and the standard mode (purple).

Fig.7.8: The PICARRO underway system is working in Fishlab.

Snow samples

From October 7th to December 3rd, 25 snow samples were collected. More specifically, 9 samples were collected from the Distributed Network floes and 16 samples were taken from the MOSAiC ice floe. For the MOSAiC floe, the snow samples were taken in parallel with the ice coring activities. Generally, the snow sample depths were on the order of 10 cm. The samples were collected using plastic gloves. After melting the samples in the lab, the water was transferred to plastic bottles (1L) and stored in the frozen container (-20℃). The snow samples will measured for $^{87}Sr/^{86}Sr$, $^{143}Nd/^{144}Nd$, $^{206}Pb/^{204}Pb$, $^{207}Pb/^{204}Pb$ and $^{208}Pb/^{204}Pb$ isotopes in the lab to trace the dust source.

Preliminary (expected) results

Picarro results

The Picarro will continue to measure the equilibrate gas from the headspace of the equilibrator. Meanwhile, the temperature of the equilibrator is recorded by a temperature sensor for calibration purposes. The methane concentration in ppm was converted to nmol/l using the temperature and salinity of the seawater from DSHIP. The time series for methane concentration, surface seawater temperature and salinity, and methane isotopes is shown in Figure 7.8.

There are 3 breaks for the methane concentration and isotopes in Figure 7.9 and 7.10. On November 5th, we calibrated the Picarro by two mixed standard gas (mixed gas 1: methane (1004 ppm, carbon dioxide (10014 ppm), mixed gas 2: methane (2 ppm),carbon dioxide (275 ppm)). On November 7th, the electronic condenser did not work well, so the water vapor was very high, so we shut down the system to fix it. On November 9th, *Polarstern* needed to release

the boiler water, so we needed to disconnect the surface sea water tubing. Therefore, we lost several hours of data.

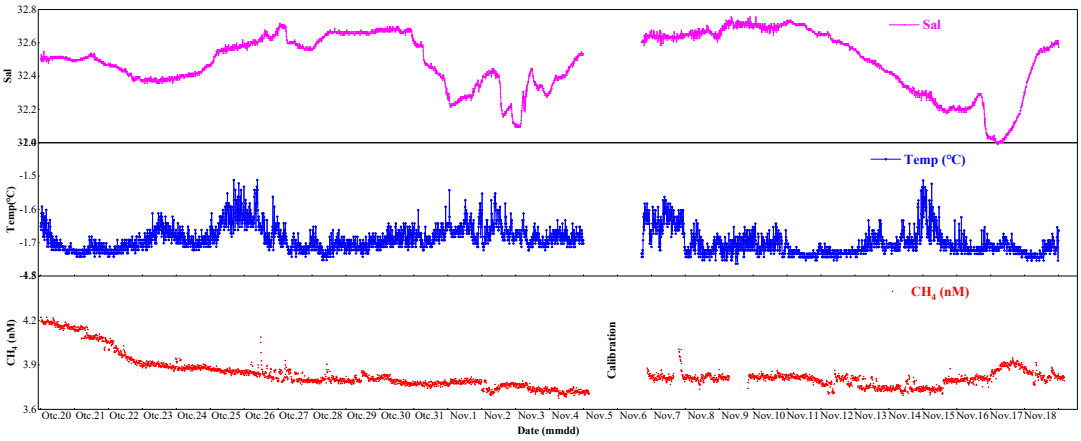

Fig.7.9: The concentration of methane, surface sea water temperature and salinity.

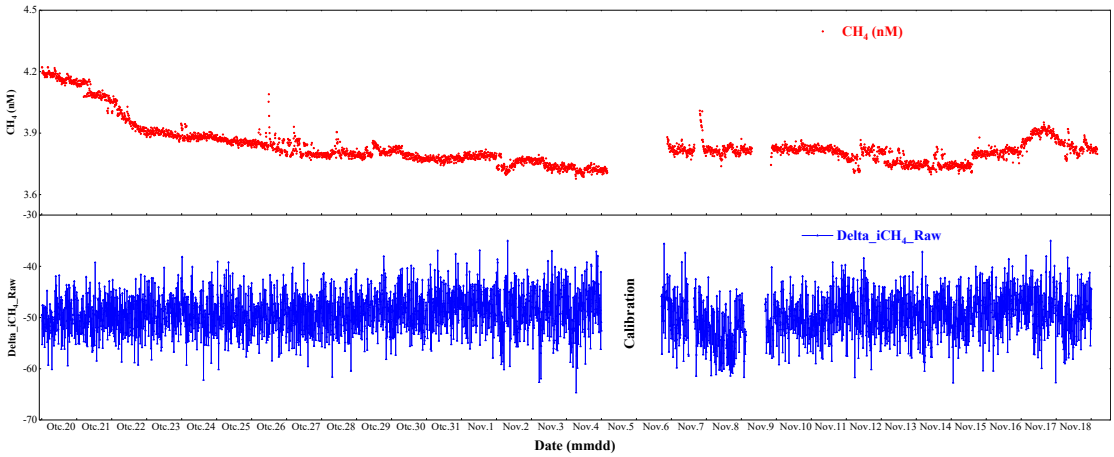

Fig.7.10: The concentration of methane and isotope.

Data Management

All data are handled, documented, archived and published following the MOSAiC data policy (see APPENDIX). Final data products will be stored at the PANGAEA data repository (World Data Center PANGAEA Data Publisher for Earth & Environmental Science (www.pangaea.de)).

References

Koch BP, Dittmar T (2006) From mass to structure: An aromaticity index for high-resolution mass data of natural organic matter. Rapid communications in mass spectrometry, 20, 926-932.

7.3 Seasonal sea ice – a new source of bromine during polar night

Katharina Abrahamsson[1] [1]SE.GU

(not on board:) A. Dumitrascu[1], P. Simoes Pereira[1], A. Saiz Lopez[2] [2]ES.CSIC

Objectives

The aim of the project is to study emissions of biologically produced trace gases, i.e. halocarbons (VHOC). These halocarbons are ozone-depleting and are hence subject to present and future regulation under international agreements (e.g., the Montreal Protocol). Although significant effort has been made to generate global budgets of halogenated compounds, the Arctic Ocean has been neglected in these models so far, hindering accurate prediction of the ozone layer over the next decades. Additionally, there is still a wide gap in knowledge in the influence of sea ice–atmosphere interactions to these halogenated compounds, especially during polar night. Changes in sea ice distribution, concentrations, and age, in the Arctic where the extent of multi-year ice has declined substantially compared to seasonal ice, affect the atmospheric composition of halogens. Halogen species involved in the depletion of ozone are associated with new sea ice formation, particularly during polar winter. For instance, during the Antarctic winter, estimates of ozone-depleting halogen fluxes from seasonal ice are 100 to 1000 times higher than during to summer (Abrahamsson *et al.*, 2018).

During the drift, we will analyse halocarbon concentrations at the ocean-ice-atmosphere interface during the Arctic winter to further our understanding of the biogeochemical processes that occur during sea ice growth, as well as their impact on Arctic tropospheric chemistry. We will also investigate the role of ice as a reaction surface for chemical conversion processes, and therefore as a source for halogens to the atmosphere. We will estimate the contribution of seasonal sea ice to the load of halocarbons in the troposphere during polar night, which will improve existing uncertainties in global flux models of halocarbons through air-ice-sea measurements.

Work at sea

Measurements of halocarbons including brominated, iodinated and chlorinated compounds, were conducted on air, sea ice, snow and seawater in order to estimate their flux, and therefore the importance of Arctic sea ice as a source for ozone-depleting halogen compounds during winter. Ice cores (triplicates) were sampled and divided into 10 cm or 5 cm sections and thawed in gas-tight Tedlar™ bags (Granfors *et al*., 2014). Snow samples were treated in a similar way. A suite of halocarbon compounds will be quantified where $CHBr_3$, CH_2Br_2, $CHCl_2Br$, $CHClBr_2$, CH_3I, CH_2ClI and CH_2I_2 are of the main interest. Samples were analyzed with a purge-and-trap system (Teledyne) connected to a gas chromatograph with electron capture detector (Thermo). A custom-made purge-and-trap instrument was equipped for semi-automatic air and seawater sample analysis. Air was continuously drawn through a ~100m long Teflon tube with a diameter of 4 mm with the help of an air pump located down-stream from the sampling loop. The instrument was also fed with a continuous stream of water from the ship´s surface water inlet. The determination was made with a gas chromatograph with an electron capture detector (Thermo). Finally, seawater was collected with the CTD/water bottle system. For sampling activities, see Tables 7.1 – 7.3.

Preliminary results

During polar springtime, active bromine drives ozone, a greenhouse gas, to near-zero levels. Bromine production and emission in the polar regions have so far been assumed to require sunlight. We have earlier reported measurements of bromocarbons in sea ice, snow and air during the Antarctic winter that revealed an unexpected new source of organic bromine to the atmosphere during periods of no sunlight. The findings were based on measurements in air, sea ice, and snow. During the drift, our hypothesis that our findings are applicable to the Arctic will also be tested.

Underway measurements:

During leg 1, approximately 2000 air and water samples were analysed for their content of halocarbons. An example of the temporal evolution of biogenic halocarbons is shown in Figure 7.11. The concentration of bromoform ($CHBr_3$) in both air and water increased during this period. In comparison, the air concentrations were in the same order of magnitude as winter air concentrations in the Weddell Sea (Abrahamsson *et al.* 2018). However, the maximum concentrations were approximately 4 times higher. The water concentrations were also higher than corresponding measurements during dark periods in the Antarctic. Also, the concentrations are approximately twice the concentrations found during summer.

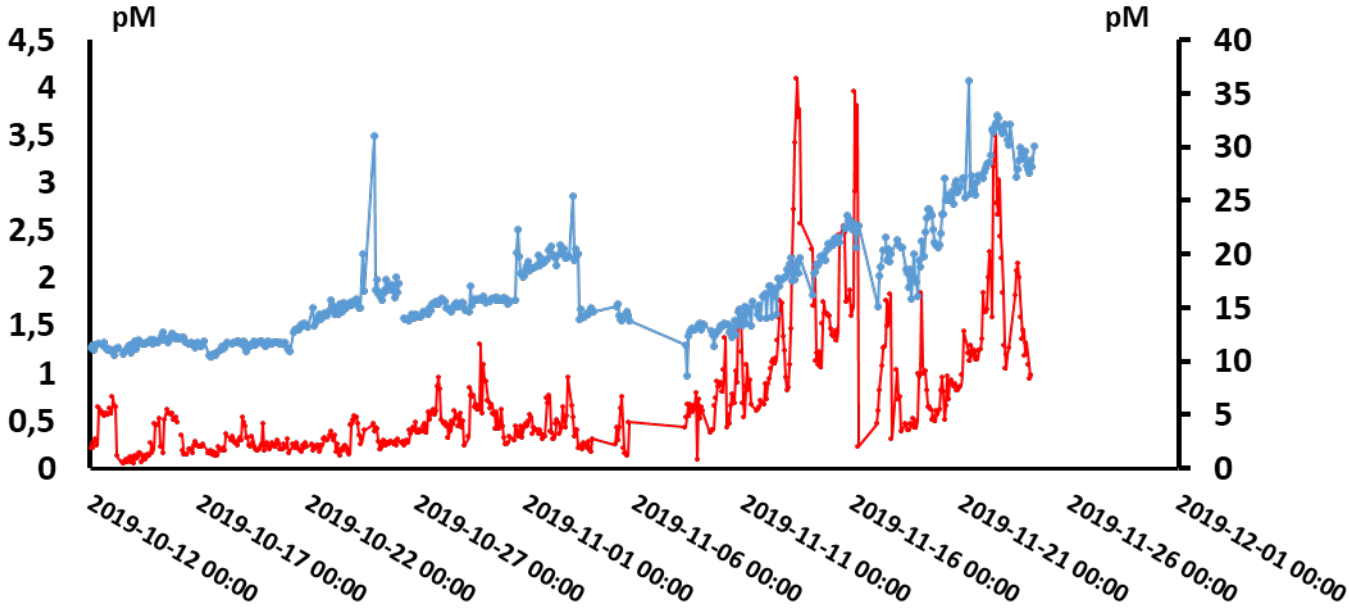

Fig.7.11: Air (red; left axis) and surface sea water concentrations (blue; right axis) of bromoform ($CHBr_3$) during leg 1. The data are not quality assured and might change.

Sea ice and snow

Halocarbon concentrations were measured in different types of sea ice. For most of the sample locations, triplicate ice cores were collected. The first-year ice at the common coring site between BGC, ECO, and ICE (Figure 7.12) had high concentrations in the upper most part with steep gradients downward. The patterns are similar to those earlier found during dark periods in the Weddell Sea indicating the same formation mechanism – a chemical reaction between bromide and ozone rather than a photochemical driven formation. The second-year ice site, which is a refrozen meltpond, showed no trends either in time or with depth in the cores. However, future work will include a comparison to physical and biological data that can help with the interpretation.

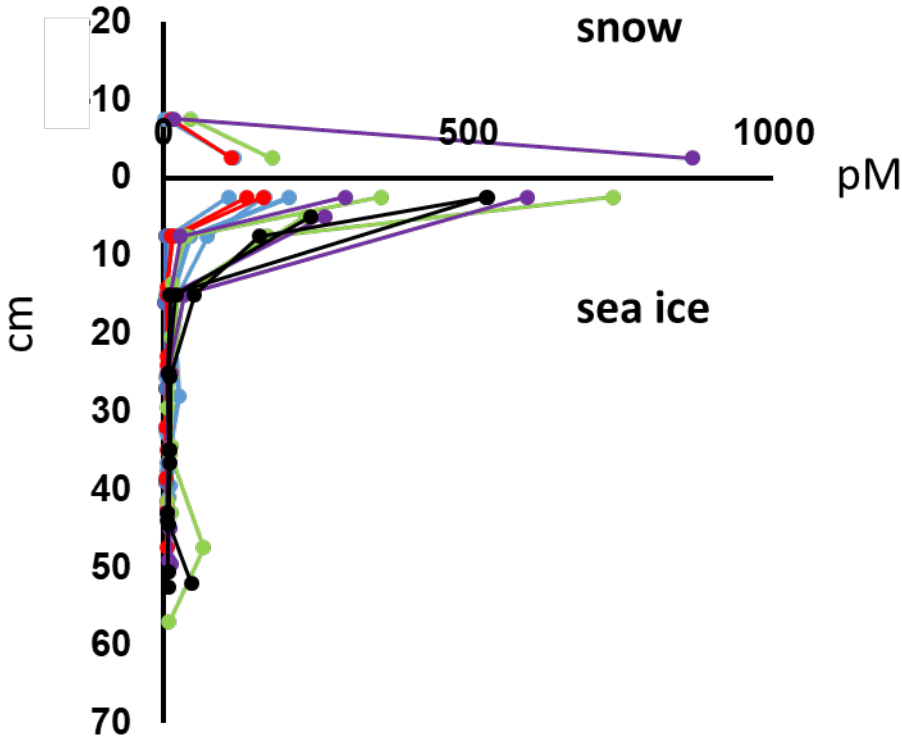

Fig.7.12: Temporal evolution of bromoform concentrations in first-year ice and snow (common coring site). The concentrations are in bulk solution and are not brine corrected. Blue: 28 Oct., Red: 4 Nov., Green: 11 Nov., Purple 18 Nov., Black: 25 Nov. The data are not quality assured and might change

Data management

All data are handled, documented, archived and published following the MOSAiC data policy (see APPENDIX). The data will be quality controlled as soon as possible after the expedition. This procedure includes inter-calibration between the two instruments. Final data products will be stored at the PANGAEA data repository (World Data Center PANGAEA Data Publisher for Earth & Environmental Science (www.pangaea.de)).

References

Abrahamsson K, Granfors A., Ahnoff M., Cuevas C.A. and Saiz-Lopez A. (2018) Organic bromine compounds produced in sea ice in Anarctic winter. Nature comm. 95291, 1-8

Granfors, A., Ahnoff, M., Mills, M. M. and Abrahamsson, K. (2014) Organic iodine in Antarctic sea ice: a comparison between winter in the Weddell Sea and summer in the Amundsen Sea. J. Geophys. Res. 119, 2276–2291